

A Kinetic Model for J-Aggregate Dynamics[†]

L. K. Gallos,[‡] A. V. Pimenov,[§] I. G. Scheblykin,[§] M. Van der Auweraer,^{||} G. Hungerford,^{||}
O. P. Varnavsky,[§] A. G. Vitukhnovsky,[§] and P. Argyrakis^{*,‡}

Department of Physics, University of Thessaloniki, 54006 Thessaloniki, Greece, Lebedev Physical Institute and Lebedev Research Center in Physics, Leninsky Prospect 53, Moscow 117924, Russia, and Laboratory for Molecular Dynamics and Spectroscopy, K. U. Leuven, Celestijnenlaan 200 F, 3001 Leuven, Belgium

Received: October 13, 1999

We developed a model to mimic the exciton dynamics in J-aggregates of cyanine dyes on the basis of Monte Carlo simulations. We consider the aggregates to be linear one-dimensional chains, where the in-phase combination of molecular excitons leads to a stabilization. A random distribution of segment lengths limits the effective coherence length and induces an inhomogeneous band broadening. The model takes into account the incoherent energy hopping between aggregates following the excitation. The results of the simulation could be fitted to the experimentally obtained absorption and fluorescence spectra and to the fluorescence decays of the J-aggregates of 3,3'-disulfopropyl-5,5'-dichloro-thiacarbocyanine (THIATS).

I. Introduction

During recent years there has been considerable interest in studies of quasi-one-dimensional structures manifesting features quite different from those in bulk of materials. In particular, J-aggregates of cyanine dyes as well as conjugated polymers, which can be approximately modeled by linear Frenkel chains, display extraordinary peculiarities in their photoresponse,^{1,2} caused mainly by the collective (excitonic) character of the excitations. A major problem in the J-aggregates is the complete assignment of the different bands and their relation to molecular packing. This relation can be elucidated to some extent by a detailed investigation of their macroscopic properties, such as absorption and emission spectra and their fluorescence decay.

Among typical J-aggregate properties are the narrow absorption and emission peaks, produced by delocalized excitonic states of the aggregate created by the electronic coupling of neighboring dye molecules, the numerous effects of the polarization of the luminescence, and unusual exciton transport properties. Though the spectral properties of these systems have been under intensive investigations for more than fifty years since the discovery of Jelly and Scheibe,^{3–5} the key structural and energetic transport properties remain unclear so far. There exist several different kinds of molecular aggregate models. In the simplest model J-aggregates^{6–8} are described as one-dimensional molecular arrays with nearest neighbor interactions. Despite its simplicity, this model accounts for most spectral properties of the aggregates with one molecule per unit cell. Other models reported in the literature^{9–12} are usually variations or extensions of this model.

The one-dimensional J-aggregate model treats the molecular aggregate as if it were a linear chain made of a large number of the aggregated coupled molecules (monomers). This is similar to the linear polymer model with the difference that the molecules are bound by van der Waals forces rather than by

chemical bonds, as polymers are. Such an aggregate structure produces a narrow peak in the absorption spectrum. Conventionally, these aggregates that reveal red-shifted absorption peaks relative to the monomer position are called J-aggregates or bathochromic, while aggregates that exhibit the blue-shifted absorption peak are called H-aggregates or hypsochromic. Though this model was widely used recently,^{13–15} no attempt was made to obtain more than the simulated absorption spectrum. In this paper we make an attempt to construct a self-consistent model of the 3,3'-disulfopropyl-5,5'-dichloro-thiacarbocyanine (THIATS) J-aggregate by simultaneous simulation of both the absorption and emission spectra, as well as the luminescence decay profiles.

II. The Model

A. Analytical Result for One-dimensional Chain. We treat the molecular aggregate within the frame of the J-aggregate model and assume that each molecule of the monomer has two states, a ground state and an excited state, and thus in the site representation the Hamiltonian of the system can be written as^{15–17}

$$H = \sum_n |n\rangle E_n \langle n| + \sum_n \sum_{m \neq n} |n\rangle V_{nm} \langle m| \quad (1)$$

Here $|n\rangle$ denotes the state in which molecule n ($n = 1, 2, \dots, N$) is excited and all others are in the ground state, E_n represents the molecular excitation energy, V_{nm} is the intermolecular interaction between molecules n and m , which is assumed to be of electrostatic origin and is often approached by a point dipole interaction.^{6,7,9,10,16} In the general case, E_n and V_{nm} vary from site to site due to diagonal and off-diagonal disorder, expressing a variation in the intermolecular interactions. Because eq 1 in general form is rather intractable, simplifying assumptions are usually made. Following the basic work of Schreiber and Toyozawa¹³ we consider the transfer energy V_{nm} to be constant, V being nonzero only between the adjacent molecules. In the simplest case when the system is not subject to any kind

[†] Part of the "Harvey Scher Festschrift" special issue.

[‡] University of Thessaloniki.

[§] Lebedev Physical Institute and Lebedev Research Center in Physics.

^{||} K. U. Leuven.

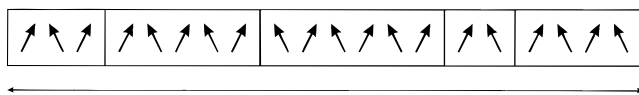


Figure 1. Schematic representation of the “broken rod” model for a 1-dimensional aggregate. The defects split the chain in segments (in this example into five segments), and each segment contains a different number N of monomers. Monomers in a segment, represented in this figure as dipoles, form a W -like structure.

of disorder, the Hamiltonian can be diagonalized in a straightforward manner, leading to the eigenfunctions

$$|\psi_k\rangle = \sqrt{\frac{2}{N+1}} \sum_{n=1}^N \sin\left(\frac{kn\pi}{N+1}\right) |n\rangle \quad (2)$$

with energies

$$E_k = E_0 + 2V \cos\left(\frac{k\pi}{N+1}\right) \quad k = 1, 2, \dots, N \quad (3)$$

The oscillator strength f_k of each transition is proportional to $\bar{\mu}_k^{*2}$ where $\bar{\mu}_k^*$ is the transition dipole to the k th level in the exciton band, and thus from eq 2 it is obvious that when k is even the oscillator strength is zero, while for small, odd k numbers it is

$$f_k \sim \mu^2 = \frac{2\bar{\mu}_{\text{monomer}}^{*2}}{N+1} \cot^2\left(\frac{k\pi}{2(N+1)}\right) \quad k = \text{odd} \quad (4)$$

where $\bar{\mu}_{\text{monomer}}^*$ is the component of the transition dipole of a monomer parallel to the aggregate axis. For $N \gg 1$ and $k = 1$, this can be approximated by

$$f_1 \sim \mu^2 = \frac{8(N+1)\bar{\mu}_{\text{monomer}}^{*2}}{\pi^2} \quad (4a)$$

Therefore, our basic equations are 3 and 4, which give the transition energies and intensities for a linear segment of N monomers in case of no disorder of any kind.

We do not attempt to calculate the intramolecular coupling and corresponding spectral shifts using the extended dipole model. Instead, we use the values of V_{mn} determined from the observed spectral shift. However, since we are simulating only the J-band, we can take into account just the lower states, which are well reproduced by the simplest one-molecule-per-unit-cell model. Thus, and since V_{mn} is negative, this simplification will not influence the density of states distribution of the exciton band in a quantitative way in the desired spectral region.

B. Disorder. The exciton energy states in J-aggregates are largely delocalized, and in an ideal aggregate they extend over the entire crystal. Because of the presence of the disorder induced by neighborhood effects and spontaneous packaging defects, there can appear an inhomogeneous distribution of the segment ground energies (diagonal disorder), and a distribution of resonance coupling constants (off-diagonal disorder).¹⁵ The presence of disorder in the chain causes energy localization, while the exciton still extends over a number of monomers. These exciton localizations can be considered as separate segments of different length, each interacting weakly between each other.

We adopt the “broken rod” model (Figure 1), which assumes that an aggregate is made of a linear sequence of segments.^{18–20} The length of these segments (which is the number of monomers N that constitute a segment) is random, accounting for the

random nature of the energy localizing disorder. Such a segment model corresponds to the transient absorption spectra of J-aggregates in both long¹⁸ and short^{21–23} pulse limits. The segments themselves are considered to be perfectly straight aggregates without any defects. Excitations are completely localized on an individual segment.

The segment length is an integer random variable, which obeys an exponential distribution characterized by a mean value N_0 , i.e.

$$P(N) = \frac{1}{N_0} \exp\left(-\frac{N}{N_0}\right) \quad (5)$$

This corresponds to the randomly broken chain of the molecules.

The excitation energies of the monomers are assumed to be all equal inside each segment and correspond to the zero order excitation energies E_0 of the segment. However, due to different local environments, the energies E_0 are subject to a Gaussian random shift, different for each segment, but the same within the particular segment. The standard deviation $\sigma_E \sqrt{N_0} / \sqrt{N}$ represents the Gaussian diagonal disorder of an N -mer aggregate, where σ_E is the standard deviation for the monomer. This parameter governs mostly the width of the red wing of the J-peak in the absorption spectrum.¹⁴ The exciton bandwidth, however, is always the same and equal to $4V$ because no nondiagonal disorder is considered here. The energies of each segment and the corresponding oscillator strengths are computed by use of equations 3 and 4 for segments of N monomers.

C. Excitation Transport Model and Algorithm. Since the state $k = 1$ bears the largest part of the oscillator strength (around 90%) and because of the rapid intrasegment relaxation, we only take into account the $k = 1$ state. At time $t = 0$, an excitation is placed in the central segment of the aggregate. After each time step the excitation moves to one of its 10 nearest neighbors (five to the left and five to the right) with probability p_i ($\sum p_i = 1$). For distances longer than 5 segments away, the transition probability, as calculated in our model, is extremely low. These probabilities are the product of two different factors denoted by W_j .

We consider the segments to interact through Coulomb operators (Förster transfer).^{10,24–26} We adopt the extended dipole approximation and W_1 becomes proportional to the square of the coupling U_i between the two segments

$$W_1 \sim U_i^2 \quad (6)$$

On each N -mer segment we assign a transition dipole

$$\frac{2\sqrt{2(N+1)}\bar{\mu}_{\text{monomer}}^*}{\pi}$$

which is no longer a point dipole but has a length equal to half the segment length, i.e., $a \cdot N/2$ where a is the length of a single dye monomer. This means that the charges at the end of the dipole equal

$$\frac{4\sqrt{2(N+1)}\bar{\mu}_{\text{monomer}}^*}{N\pi a} \approx \frac{4\sqrt{2}\bar{\mu}_{\text{monomer}}^*}{\sqrt{N}\pi a}$$

taking into account eqs 4 and 4a. The coupling U_{ij} is given by the electrostatic interactions among the four charges of the two interacting dipoles. Furthermore, we assume the N -mers arrangement geometry given in Figure 1. As numerical calculations suggested, the values of U_{ij} are close to those calculated

using a point dipole model. The coupling between aggregates of the same coherence length N_i will be proportional to $N_i^{1/2} N_j^{1/2}$ divided by the cube of the distance between the centers. As the latter is proportional to N_i , U_{ij} will be proportional to N_i^{-2} .

The rate of exciton migration will also be influenced by energetic effects, which we can reduce to a thermal factor W_2 (Boltzmann effect). We calculate the energy difference between the two interacting segments: $\Delta E = E_{\text{neighbor}} - E_i$, where the energy of an N-mer segment is given by

$$E_k = E_0 - 2V \cos\left(\frac{k\pi}{N+1}\right) \quad (7)$$

since we always consider $k = 1$. We use the standard Monte Carlo^{23,27} criterion depending on whether the energy difference is favorable or not, and W_2 is given by

$$W_2 \sim \begin{cases} e^{-\Delta E/kT} & \Delta E > 0 \\ 1 & \Delta E \leq 0 \end{cases} \quad (8)$$

Although this criterion was originally developed for electron transfer, it can be generalized for other nonadiabatic processes (e.g., energy transfer) whose rate is governed by the golden rule.²⁸ The value of the intermolecular coupling V was estimated from the fact that the J-aggregate band, in the presumption of the infinite segment length, should be shifted from the monomer position to the value of 16100 cm^{-1} , since the total bandwidth of the excitonic band should be according to eq 3 given by $4V$. Therefore, this value has been fixed to $V = 770 \text{ cm}^{-1}$, and the lattice size to 400 sites. We examined the behavior of $\langle N \rangle$, as a function of N_0 , σ , and T . This value of 770 cm^{-1} , which has been determined experimentally from the spectral shift of the J-aggregate band, corresponds to theoretical values calculated for a similar dye using a transition density of a CNDO formalism.^{29–31}

According to eqs 1 and 3, the electronic matrix element between two aggregates with aggregation number $N_i = N_j = N$ is given in a naive point dipole approximation by

$$U_{ij} N_i^{1/2} N_j^{1/2} = \frac{N_i^{1/2} N_j^{1/2} \mu_M^{*2}}{4\pi\epsilon_0 \left(\frac{N_i + N_j}{2}\right)^3 a^3} \approx \frac{\mu_M^{*2}}{4\pi\epsilon_0 N^2 a^3} \quad (9)$$

where a is the intermolecular distance, μ_M^{*2} the transition dipole of a monomer, and ϵ_0 the permittivity of vacuum ($8.85 \times 10^{-12} \text{ C}^2/\text{Vm}$). Using $5.97 \times 10^{-30} \text{ Cm}$ for μ_M^* ,^{32–34} $3.66 \times 10^{-10} \text{ m}$ for a , 10 for N_i and N_j , we obtain as an upper limit for the electronic factor for $U_{ij} N_i^{1/2} N_j^{1/2} = 6.5 \text{ cm}^{-1}$. Using the extended dipole approximation and taking into account Franck–Condon factors will further reduce the matrix element. This matrix element is 2 orders of magnitude smaller than the disorder or the thermal energy both at 77 and 287 K (50 and 200 cm^{-1}). Hence the hopping rate can be described in the framework of a golden rule. Therefore, the probability of hopping to a specific segment is determined by the relation $p_i = W_1 W_2$. In the present approach, all p_i 's are normalized by their sum $\sum p$. We divide the unit interval to segments of length equal to these probabilities $p_i / \sum_k p_k$. The choice of the exciton move is performed by drawing a random number. This number falls in a segment, which corresponds to a specific probability, and the excitation moves to this N-mer. This procedure is considered to consume one time unit, equivalent to one Monte Carlo step. The excitation makes a move in every step, i.e., there is no probability for it to stay on the same segment. In this picture the time unit is a

mean value of all possible hopping times the excitation can perform. The excitation, in general, may require a variable time interval in order to perform a jump and to stay on a particular segment. Since we cannot describe these hops in detail we consider that each hop lasts a mean constant time. It includes both the residence time and the time needed for the hop, and we call it ‘‘hopping time’’. In the computational model, one Monte Carlo step is exactly the same as one unit of this hopping time.

We have also taken into account the natural lifetime of the excitation and thus introduced a finite probability for the excitation to decay. At each time step there are two options: either the excitation decays or chooses to move to an adjacent site, with the algorithm described above. The probability of decay depends on a decay constant d and is equal to Nd , where N is the segment length. Therefore, the first decision made is whether the excitation will decay. This is done by comparing a random number to the product Nd . If the outcome is favorable for decay the motion of the excitation stops and we repeat the whole procedure with another excitation. If it continues to exist it uses the above-mentioned Monte Carlo algorithm and moves to a neighboring site, where again we check for decay, and so on.

III. Experimental and Simulation Procedures

A. Experimental. The triethylammonium salt of 3,3'-disulfopropyl-5,5'-dichlorothiacyanine iodide (THIATS) was obtained by courtesy of AGFA N. V. For preparation of the molecular aggregate THIATS was dissolved in a 3:2 v/v water/ethylene glycol (WEG) mixture upon heating to $60 \text{ }^\circ\text{C}$. The solutions with dye concentration of 10^{-4} to 10^{-3} M were cooled to room temperature, put into a dismantable glass cell 300 mm in thickness, then cooled and kept at 250 K for about 10 min. At this stage a narrow red-shifted J-band appeared in the absorption spectrum. The samples were then quickly frozen in liquid nitrogen and placed into a nitrogen or helium cryostat. To measure the absorption spectra, the Jobin–Yvon polychromator coupled with the PAR OMA-2 optical multichannel analyzer was used. For the lifetime measurements the Edinburgh Instruments time-correlated single-photon counting setup with the time resolution of 54 picoseconds was used.

B. Numerical Investigation of the Exciton Random Walk.

At first, we view the exciton transfer as a simple diffusion process modeled by a random walk. We thus monitor $\langle R^2 \rangle$, the mean squared displacement, as a function of time.

In Figure 2 we show $\langle R^2 \rangle$ versus time for five different temperatures $kT = 1, 5, 20, 200$, and 350 cm^{-1} (equivalently, $T = 1.4, 7.2, 28.6, 287$, and 500 K). The lines are the result of the average of 10000 different realizations. The classical prediction with no disorder would give $\langle R^2 \rangle = t$. As we see in Figure 2, the effect of temperature is important only in the region of low temperatures. As we raise the temperature the thermal energy becomes of the same magnitude as the difference of the excitation energy of two neighboring segments ($2V\pi\sigma/N \langle N \rangle^3$), and this factor is no longer affecting the decisions anymore, allowing the Forster factor to predominate. Thus, at higher temperatures the classical random walk is recovered. We also observe that at low T the system is highly nonlinear, which is expected when one considers the above thermal factors.

Another quantity of interest is the aggregation number N of the segment where the excitation is found after t time steps, and especially whether the excitation prefers segments of large or small N . By fixing the time t and performing several different realizations of the walk, typically of the order of 10000 runs,

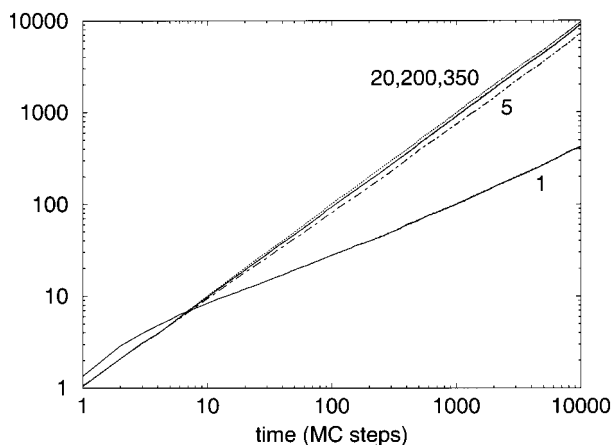


Figure 2. Mean squared displacement for the excitation random walk on the disordered chain. Five different temperatures kT are presented, as marked: $kT = 1, 5, 20, 200, 350 \text{ cm}^{-1}$. The curves for the higher temperatures are practically indistinguishable. We use an exponential length distribution with a mean segment length $N_0 = 10$.

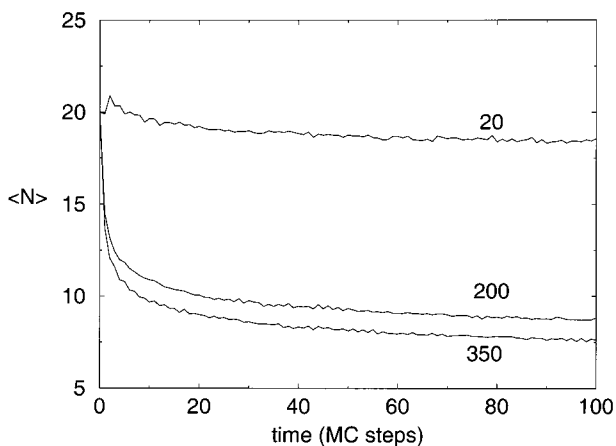


Figure 3. Evolution of $\langle N \rangle$ with time for three different temperatures $kT = 20, 200, \text{ and } 350 \text{ cm}^{-1}$ for an exponential segment length distribution with mean segment length $N_0 = 10$.

we can construct the histogram $P(N,t)$, which gives the probability of finding the excitation at time t on a segment of length N . From such histograms we can evaluate the mean value of the segment length $\langle N \rangle$ as a function of time for different sets of parameters. This mean value is given by

$$\langle N \rangle_t = \sum_N NP(N,t) \quad (10)$$

and can be considered as a measure of the total emission intensity at time t due to the proportionality of the fluorescent rate constant with N . We observe that the mean values of the segment lengths $\langle N \rangle$ are shifted toward shorter segment lengths than N_0 . This could be explained by the fact that since our ensemble has exponential distribution of the segment lengths, the short segments dominate in the segment size spectrum. It is worth mentioning here that our model does not take into account the possibility of the exciton trapping. Even though longer segments possess lower energy, on the next time step the exciton is forced to move to one of the nearest segments. We should stress, however, that the exciton transport in our model is governed mostly by the Förster factor rather than the thermal one.

In Figure 3 we present $\langle N \rangle_t$ versus time for $N_0 = 20$. Three different temperatures are presented, namely $kT = 20, 200, 350$

cm^{-1} . We notice that, independent of the temperature, the mean value of N is shifted asymptotically toward shorter segment lengths. For $kT = 20 \text{ cm}^{-1}$ the $\langle N \rangle$ value is always larger than that for higher temperatures, because the thermal factor is an additional obstacle for the excitation to move toward a smaller segment.

C. Simulation of the Spectra. The absorption spectrum can be calculated by applying the standard procedure of calculating the eigenenergies and the corresponding oscillator strengths.^{13,14} We generate random chains by using an exponential distribution for the segment lengths. Equations 3 and 4 indicate the energies where these chains absorb and the corresponding absorption intensity. We construct the absorption spectrum by using a binning technique, where the width of each bin is equal to 1 cm^{-1} . Every time we determine an absorption line for a particular chain we add the value of its oscillator strength to the corresponding bin. Upon repeating this procedure for a large number of chains we gradually build a histogram, which is the absorption spectrum. We then peak-normalize to 1 in order to compare this to the experimental spectrum.

To construct the emission spectrum we need to also take into account the finite lifetime of an excitation. For each de-excitation a photon is emitted, and we add this to the energy corresponding to its wavelength with the appropriate oscillator strength. The energy and the oscillator strength are computed for the N -mer on which the excitation was located at the time that it decayed. The histogram is then built the same way as described for the absorption spectrum.

Finally, we simulated the time-dependent fluorescence decays of THIATS. Experimentally, this curve is acquired by a single-photon counting technique. A monochromator window is placed on the peak of maximum intensity. We use the exact same algorithm for the transfer process as in the case of the emission spectrum. However, we now construct a temporal histogram. We monitor the time needed for an excitation to decay. When it finally decays we store the “existence time”. Different realizations of the system allow us to construct a histogram, where the x -axis represents the time and the y -axis the percentage of excitations decaying at that particular time. Finally, we perform a convolution of the derived function with the instrumental response function. By varying the values of the hopping time, i.e., the time which corresponds to one Monte Carlo step, we can stretch or compress the curve along the x -axis. In this way we can determine which values of the hopping time yield a better description of the experimental fluorescence spectrum. Note that an excitation which decays is only recorded when its energy falls within the frequency interval of the monochromator window. Otherwise, it is ignored because it would not have been recorded experimentally.

IV. Results and Discussion

In our effort to construct the absorption spectrum of THIATS aggregates we varied all of the relevant parameters and found out that the parameters which yield the best fittings are $N_0 = 8$, $\sigma_E = 60 \text{ cm}^{-1}$ (disorder of the exciton band center position), and the energy level of the monomer should be 17500 cm^{-1} . The absorption spectra (experimental and computed) are presented in Figure 4. We can see that the coincidence between the two curves is indeed very good. There was no need to introduce the χ^2 or any other statistical indicator because the estimation of the fitting parameter within 10% is sufficient for this qualitative work.

The result of the simulation of the emission spectrum is shown in Figure 5. Ideally, one would like to calculate the emission

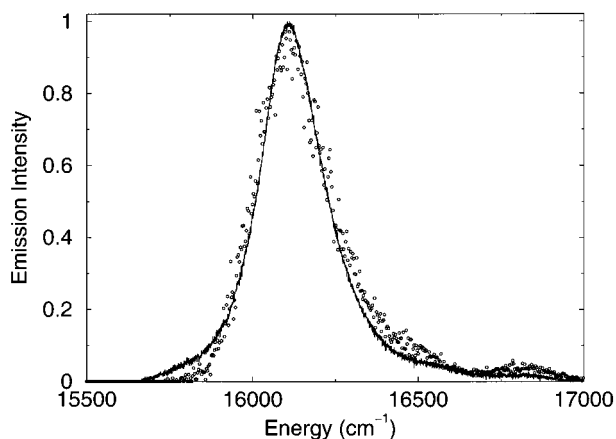


Figure 4. Simulation of the absorption spectrum of THIATS (dashed line) and comparison to the experimental spectrum (solid line). Parameters used: $N_0 = 8$, $\sigma_E = 60 \text{ cm}^{-1}$, $E_0 = 17500 \text{ cm}^{-1}$.

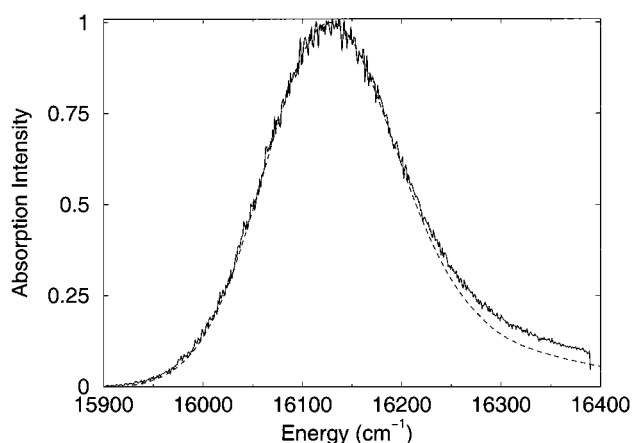


Figure 5. Simulation of the emission spectrum of THIATS (symbols) and comparison to the experimental spectrum (solid line). Parameters used: $N_0 = 9$, $\sigma_E = 90 \text{ cm}^{-1}$, $E_0 = 17600 \text{ cm}^{-1}$, and $d = 5 \cdot 10^{-6}$.

spectrum with the exact same parameters as for absorption. However, we have found that the best fit corresponds to $N_0 = 9$, $\sigma_E = 90 \text{ cm}^{-1}$, and $E_0 = 17600 \text{ cm}^{-1}$. The decay constant is equal to 5×10^{-6} . The main difference is in the width of the two spectra, since experimentally it is found that the emission spectrum is much wider than the absorption one.

The simulated decay curves are shown in Figure 6 in comparison to the experimental decays. The best fit is found when we consider a hopping time of 0.1 ps and a decay constant $d = 5 \times 10^{-6}$. This small hopping time correlates with the extremely high mobility of excitons in such systems as it is seen from the exciton–exciton annihilation experiments.³⁵

Note that all results were obtained assuming that the excitation is not producing more than one exciton per aggregate cluster, meaning that only one segment of the aggregate chain is excited. This means that the excitation intensity used in the experiments related to the analogous simulations should be weak enough. Otherwise, the model proposed should take into account the more complex multiexciton processes such as exciton–exciton annihilation.³⁵ This latter process is under current investigation.

V. Conclusions

When exciting a mesoscopic³⁶ J-aggregate consisting of a large number of segments of exponentially distributed length, a rapid (4 ps) redistribution of the excitation energy over the assembly occurs. This suggests that the nonexponential decays occurring in a time range between 100 ps and 1 ns, observed

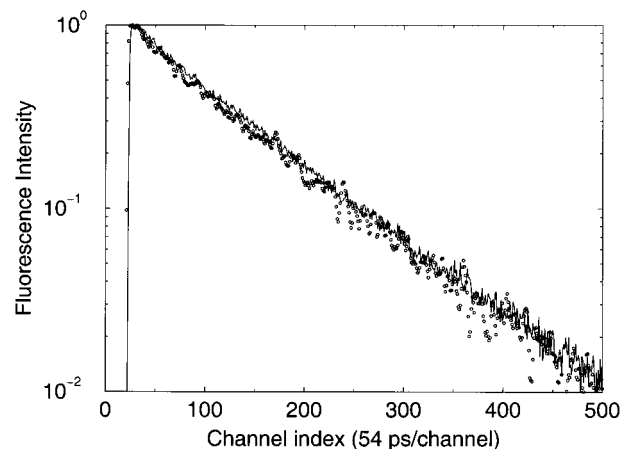


Figure 6. Simulation of the time-dependent fluorescence decay curves of THIATS (symbols) and comparison to the experimental spectrum (solid line). The x -axis is presented in channel index, where each channel corresponds to 54 ps. Parameters used: hopping time = 0.1 ps, $N_0 = 9$, $\sigma_E = 90 \text{ cm}^{-1}$, $E_0 = 17650 \text{ cm}^{-1}$, and $d = 5 \cdot 10^{-6}$.

frequently in the analysis of J-aggregate fluorescence decays,^{32–34} are probably not related to this redistribution process.

Around room temperature, electronic factors appearing in the expression for the rate of energy transfer determine the final pseudostationary distribution, characterized by an average coherence length approaching $\langle 1/N \rangle^{-1}$. At low temperature, energetic factors also become important.

Although the model used contains several simplifications concerning both the calculation of the energy of the aggregates and the simulation of the exciton hopping process, the results of simulating the spectra are very satisfactory. As the parameter V is not calculated a priori but used as an experimentally determined (fitted) parameter, the simplifications used will have no direct effect on the results presented here. Simulations using either the point dipole or more extensive expressions show that, except for H-aggregates, the nonnearest neighbor interactions are generally more than five times smaller than the nearest neighbor interactions.

In the simulations of the exciton transport we observed that at room temperature, where energetic aspects are probably not relevant, energy transfer results in a pseudostationary value of $\langle N \rangle$, which is significantly smaller than the characteristic aggregate size N_0 (which is the average value of the exponential distribution). The smaller lengths are preferred mainly because of their much higher probability of occurrence, compared to larger segments whose probability of occurrence decreases exponentially. Additionally, in our model, the energy difference between segments of similar lengths is not significant and generally it is comparable to the thermal energy.

Although we have not attempted to perform a simulation of the entire set of the luminescent properties of the molecular aggregates of the THIATS dye, we have shown that some information on the parameters of the luminescent states of such systems can be obtained even by use of this simple model. The actual nature of these states remains unknown, and the complete details of the energy transport mechanism are still under discussion.

Acknowledgment. The authors thank RFBR for support of this work through grants 96-02-16527 and 96-15-96763, and INTAS for the grant 85-93. A.V.P. and I.G.S. also thank the ISSEP for its support. M.V.d.A. is a “Onderzoeksdirecteur” of the F.W.O.-Vlaanderen. G.H. thanks the research Council of the K.U. Leuven for a Junior Fellowship. The authors gratefully

acknowledge the FWO-Vlaanderen, the Flemish Ministry of Education for the support through GOA/1/96 and the support from DWTC (Belgium) through IUAP-IV-11. Finally, the support of NATO grant SFP-971940 is gratefully acknowledged.

References and Notes

- (1) Spano, F. C.; Knoester, J. In *Advances in Magnetic and Optical Resonance*; Warren, W. S., Ed.; Academic: New York, 1994; Vol. 18, p 117.
- (2) Knoester, J.; Spano, F. C. In *J-Aggregates*; Kobayashi, T. Ed.; World Scientific: Singapore, 1996.
- (3) Jelly, E. E. *Nature* **1936**, *138*, 1009.
- (4) Scheibe, G. *Angew. Chem.* **1936**, *49*, 563.
- (5) Scheibe, G. Lage, Intensität und Struktur von Absorptionbanden; In *Optische, Anregungenorganischer Systeme*; Foerst, W., Ed.; Verlag Chemie: Weinheim, 1966; p 109.
- (6) Kasha, M. *Rev. Mod. Phys.* **1959**, *31*, 1.
- (7) Kasha, M. *Radiat. Res.* **1963**, *20*, 55.
- (8) Mac Rae, E. G.; Kasha, M. The Molecular Exciton Model in *Physical Processes in Radiation Biology*; Academic Press: New York, 1964; pp 23–42.
- (9) Czikkely, V.; Dreizler, G.; Forsterling, H. D.; Kuhn, H.; Sondermann, J.; Tillman, P.; Wiegand, J. *Z. Naturforsch.* **1969**, *24a*, 1823.
- (10) Czikkely, V.; Försterling, H. D.; Kuhn, H. *Chem. Phys. Lett.* **1970**, *6*, 207.
- (11) Hochstrasser, R. *Photochem. Photobiol.* **1965**, *3*, 317.
- (12) Kato, T.; Sasaki, F.; Kobayashi, A. S. *Chem. Phys.* **1998**, *230*, 209–221.
- (13) Schreiber, M.; Toyozawa, Y. *J. Phys. Soc. Jpn.* **1982**, *51*, 1528, 1544.
- (14) Argyrakis, P.; Basko, D. M.; Drobizhev, M. A.; Lobanov, A. N.; Pimenov, A. V.; Varnavsky, O. P.; Auweraer, M.; Vitukhnovsky, A. G. *Chem. Phys. Lett.* **1997**, *268*, 372.
- (15) Fidler, H.; Knoester, J.; Wiersma, D. A. *J. Chem. Phys.* **1991**, *95*, 7880.
- (16) Davydov, A. S. *Theory of Molecular Excitons*; Plenum: New York, 1971.
- (17) Knapp, E. W. *Chem. Phys.* **1984**, *85*, 73.
- (18) Durrant, J. R.; Knoester, J.; Wiersma, D. A. *Chem. Phys. Lett.* **1994**, *222*, 450.
- (19) Möll, J.; Dahne, S.; Durant, J. R.; Wiersma, D. A. *J. Chem. Phys.* **1995**, *102*, 6362.
- (20) Makhov, D. V.; Egorov, V. V.; Bagatur'yants, A. A.; Alfimov, M. V. *Chem. Phys. Lett.* **1995**, *245*, 371.
- (21) Spano, F. C. *Chem. Phys. Lett.* **1994**, *220*, 365.
- (22) Spano, F. C. *Chem. Phys. Lett.* **1995**, *234*, 29.
- (23) Spano, F. C. *Chem. Phys. Lett.* **1995**, *234*, 354.
- (24) Kuhn, H. *J. Chem. Phys.* **1970**, *53*, 101.
- (25) Förster, Th. In *Modern Quantum Chemistry Part IIIB*; Sinanoglu, O., Ed.; Academic Press: New York, 1965; pp 93–127.
- (26) Möbius, D.; Kuhn, H. *Isr. J. Chem.* **1979**, *18*, 375.
- (27) Miller, A.; Abrahams, E. *Phys. Rev.* **1960**, *120*, 745.
- (28) Blumen, *Chem. Phys. Lett.* **1980**, *70*, 387–391.
- (29) Asunama, H.; Ogawa, K.; Fukunaga, H.; Tani, T.; Tanaka, J. *Proceedings of the ICPS 1998 International Congress on Imaging Science*; Antwerp, Belgium, 1998; pp 178–182.
- (30) Rosenoff, A. E.; Norland, K. S.; Ames, A. E.; Walworth, V. R.; Bird, G. R. *Phot. Sci. Eng.* **1968**, *12*, 185–195.
- (31) Norland, K.; Ames, A.; Taylor, T. *Phot. Sci. Eng.* **1970**, *14*, 295.
- (32) Scheblykin, I. G.; Drobizhev, M. A.; Varnavsky, O. P.; Van der Auweraer, M.; Vitukhnovsky, A. G. *Chem. Phys. Lett.* **1996**, *261*, 181.
- (33) Scheblykin, I. G.; Drobizhev, M. A.; Varnavsky, O. P.; Vitukhnovsky, A. G.; Van der Auweraer, M. *Chem. Phys. Lett.* **1998**, *282*, 250–256.
- (34) Auweraer, M.; Hungerford, G.; Vranken, N.; Gretchikine, A.; De Schryver, F. C.; Scheblykin, I. G.; Varnavsky, O.; Vitukhnovsky, A. In *Proceedings of the ICPS International Congress on Imaging Science*; Antwerp, Belgium, 1998; Vol 1, pp 174–177.
- (35) Sundstrom, V.; Gillbro, T.; Gadonas, R. A.; Piskarskas, A. *J. Chem. Phys.* **1988**, *89*, 2754.
- (36) Misawa, K.; Kobayashi, T. *J-Aggregates*; Kobayashi, T., Ed.; World Scientific Publishing: Singapore, 1996; p 41.